Master's Thesis

# Facile in-situ fabrication of target amplified reusable 3D hydrogel Surface-Enhanced Raman spectroscopy (SERS) platform in microfluidic system

Yoonkyung Shin

Department of Chemical Engineering

Graduate School of UNIST

2020

# Facile in-situ fabrication of target amplified reusable 3D hydrogel Surface-Enhanced Raman spectroscopy (SERS) platform in microfluidic system

Yoonkyung Shin

Department of Chemical Engineering

Graduate School of UNIST

# Facile in-situ fabrication of target amplified reusable 3D hydrogel Surface-Enhanced Raman spectroscopy (SERS) platform in microfluidic system

A thesis/dissertation

submitted to the Graduate School of UNIST

in partial fulfillment of the

requirements for the degree of

Master of Science

Yoonkyung Shin

07/05/2020 of submission

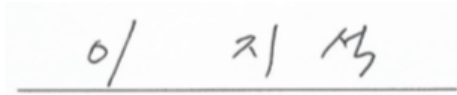Approved by

_____

Advisor

Jiseok Lee

# Facile in-situ fabrication of target amplified reusable 3D hydrogel Surface-Enhanced Raman spectroscopy (SERS) platform in microfluidic system

Yoonkyung Shin

This certifies that the thesis/dissertation of Yoonkyung Shin is approved.
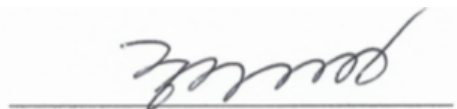
07/05/2020 of submission

signature

Advisor: Jiseok Lee

signature

Hyunhyub Ko: Thesis Committee Member #1

signature

Seok Ju Kang: Thesis Committee Member #2

# Abstract

The surface enhanced Raman scattering (SERS) effect is a promising technique to acquire molecular information. However, in order to achieve high enhancement factor as well as homogeneous Raman signal, the methods developed so far have limitation in that it requires complex, costly, and time-consuming processes. In this study, we integrated SERS and microfluidic device by in-situ growth of silver nanoparticles in hydrogel micro-posts array via automated digital micromirror device (DMD)-based maskless flow lithography technique. The hydrogel-based SERS system in microfluidic channel allowed target molecules amplification effect and real-time detection. In addition, the 3D porous hydrogel network not only enabled compact density of Ag NPs within overall hydrogel structure but also easily removed the target molecules after Raman measurement, providing high sensitivity and reusability capability. In addition, the SERS substrate was proven to be highly reproducible by measuring Raman signal from randomly selected spots and the Raman mapping images of a single hydrogel micro-post. Lastly, real-time detection of date drug was carried out in the presence of alcohol for practical application.

# Contents

# List of Figure

DMD-based maskless flow microlithograpy technique. (B) Fabrication process of reusable hydrogel-based SERS platform. (i) Electrostatic interaction between Ag ions and carboxylic groups of acrylic acid after incubation of $AgNO_3$ solution. (ii) In-situ growth of Ag NPs in hydrogel structure by photoreduction of Ag ions by 365 nm UV light. (iii) Removal of blue Ag NPs with 30 vol.% PEG200 solution. (iv) SERS measurement by target amplification process.

**Figure 8.** Schematic illustration of the UV LED installed DMD microlithography system.

**Figure 9.** (A) Bright field images and (B) UV-Vis absorption spectra of Ag NPs hydrogel micro-posts array according to the 365 nm UV exposure time. The 4× magnification images at the top and 20× magnification images at the bottom. Scale bars are 100 μm and 50 μm, respectively.

**Figure 10.** (A) Bright field optical micrographs of hydrogel micro-post fabricated without AA exposed to the UV light for a varying amount of time after infused with the metal precursor solution. (B) UV-Vis absorption spectra of PEGDA hydrogel micro-post fabricated with and without AA.

**Figure 11.** (A) Bright field images and (B) UV-Vis absorption spectra of Ag NPs hydrogel micro-posts array after rinsing with 30 vol.% PEG 200 solution in DI water. The 4× magnification images at the top and 20× magnification images at the bottom. Scale bars are 100 μm and 50 μm, respectively.

**Figure 12.** HRTEM images of (A) 1min Ag NPs with LSPR band at 622 nm, Ag NPs with LSPR band at 430 nm (B) before and (C) after rinsing with PEG200.

**Figure 13.** Energy-dispersive X-ray spectroscopy (EDS) spectra of hydrogel micro-posts with LSPR band at (A) 622 nm (blue Ag NPs) and (B) 430 nm (yellow Ag NPs)

**Figure 14.** Bright-field images of (A) PEGDA, (B) PEGDA/AA and, (C) PEGDA/AA/Ag hydrogel micro-posts array immersed in 1 μM of R6G. (D) UV-Vis absorption spectra and (E) Raman shift of 1 μM of R6G solution and hydrogel micro-posts of PEGDA, PEGDA/AA, and PEGDA/AA/Ag post immersed in 1 μM of R6G.

**Figure 15.** The normal Raman spectrum of aqueous $10^{-1}$ M R6G molecules adsorbed on PEGDA

post enlarged by 10 times (Excitation wavelength: 633nm, Integration time: 1sec).

**Figure 16.** (A) Raman spectra of the PEGDA/AA/Ag micro-post array and (B) average Raman intensities measured at 773 cm$^{-1}$ and 1508 cm$^{-1}$ are shown. The error bars indicate the standard deviations calculated for measurements of 10 independent samples.

**Figure 17.** The reliability and reproducibility of measurements for R6G by the PEGDA/AA/Ag micro-posts. For ten different spots within a single micro-post immersed in the 10 μM R6G aqueous solution, (A) the entire Raman spectra and (B) the standard deviations of Raman intensities measured at each peak position are shown. (C) the entire Raman spectra and (D) the standard deviations of Raman intensities calculated at three peak positions for each of three microfluidic devices were shown. For nine different spots in each of the micro-posts from three individual microfluidic devices, *i.e.* a total of 27 spots.

**Figure 18.** A series of in-plane mapping of the Raman intensity measured at 1508 cm$^{-1}$ along the thickness direction. A distance between adjacent in-plane mapping is 2 μm.

**Figure 19.** Confocal Raman mapping images of 10 μM of R6G concentration in single PEGDA/AA hydrogel micro-post. Mapping images are constructed based on Raman peak of PDMS at 830 cm$^{-1}$ (red) and glass slide at 1400 cm$^{-1}$ (yellow) band. The point to point mapping distances in X, Y, and Z directions are 5, 5, and 2.5 μm, respectively. No R6G peak was observed in the hydrogel post without Ag NPs.

**Figure 20.** The reusability, continuous multi-target sensing capability, and a demonstration of the practical application of the PEGDA/AA/Ag micro-posts. (A) Bright-field optical micrographs, (B) Raman spectra, and (C) Raman intensity measured at 1508 cm$^{-1}$ were observed as the microfluidic device was injected alternatively with the 10 μM R6G aqueous solution and the methanol – a washing solvent – for five minutes for each fluid. The cycle was repeated for 20 times consecutively. A scale bars is 100 μm.

**Figure 21.** (A) SERS spectra of GHB (5.0 M) and 40 % EtOH in PEGDA/AA/Ag micro-posts and Raman spectra of GHB (5.0 M) in PEGDA/AA micro-posts. (B) The Raman spectra of the PEGDA/AA/Ag micro-posts for a varying concentration of GHB in the ethanol solution.

**Figure 22.** (A) The effect of washing solvent on recovering the pristine state of the

PEGDA/AA/Ag micro-post after the initial measurement of *p*-ABA. (B) Sequential and continuous measurements of *o*-, *m*-, and *p*-ABA with the intermittent washing by the methanol. The order of measurement is downward.

# List of Table

**Table1.** Comparisons of the substrate materials, enhancement factor of R6G, sample preparation, reusability, and targets detected between our work and previous ones.

# Nomenclature

_____

**SERS** Surface enhanced Raman spectroscopy

**LSPR** Localized surface plasmon resonance

**DMD** Digital micro-mirror device

**AgNO₃** Silver nitrate

**Ag** Silver

**Ag NPs** Silver nanoparticles

**AA** Acrylic acid

**UV-Vis** Ultraviolet-visible

**EDS** Energy dispersive spectrometer

**HR-TEM** High-resolution transmission electron microscopy

**EF** Enhancement factor

**PEGDA** Polyethylene glycol diacrylate

**PEG200** Polyethylene glycol 200

**MeOH** methanol

**EtOH** ethanol

**DI water** deionized water

**R6G** Rhodamine 6G

**GHB** γ-hydroxybutyric acid

**ABA** Aminobenzoic acid

_____

# I. INTRODUCTION

## 1.1 Surface Enhanced Raman Spectroscopy (SERS)

Raman scattering is an inelastic scattering of photons that occur when incident photon and molecules interact each other, resulting in energy gains or loses. Even though, Raman spectroscopy is a promising spectroscopy technique which provides molecular specific information by the vibrational modes of the molecules, the very low Raman scattering cross-sections resulted in limited detection of molecules at low concentration (**Figure 1A**). To overcome these limits, surface-enhanced Raman scattering (SERS) has been studied to provide the enhanced sensitivity of Raman signals. The inherently weak Raman signal can be enhanced using the strongly localized electric fields via collective oscillations of conducting electrons on the surface of metallic nanostructures such as silver (Ag), gold (Au) and copper (Cu).[1] (**Figure 1B**). SERS has been used in a wide range of research fields such as biology,[2, 3] chemistry,[4] and the environment[5] by the great advantages of label-free and non-destructive analyte detection. For highly enhanced SERS signal, nanostructure morphologies, gap between metallic nanoparticles, and distance between analyte and plasmonic surface are considered important.
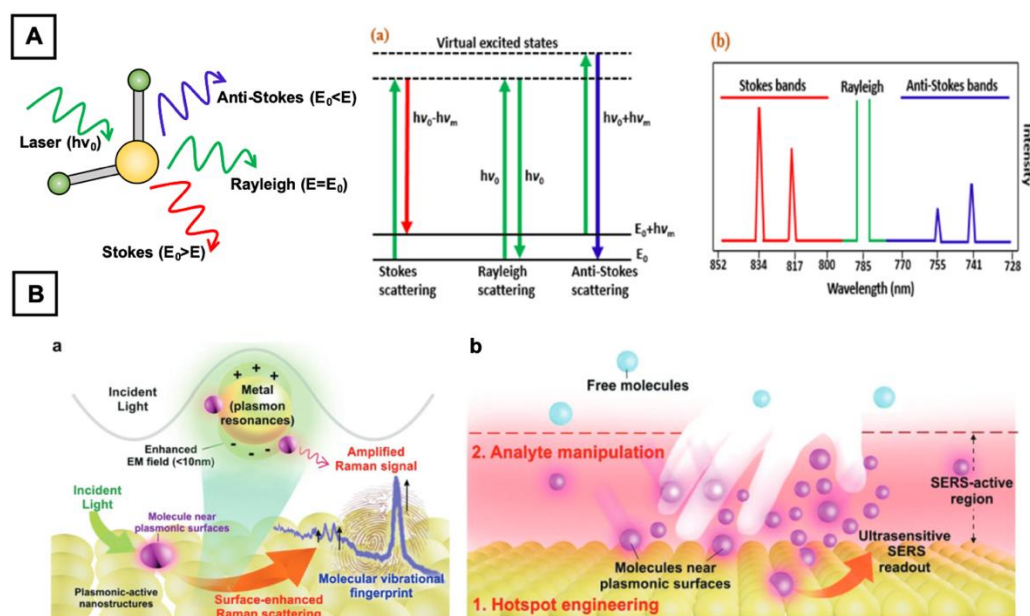


**Figure 1. (A)** Schematic representation of Rayleigh and Raman scattering. (Lohumi et al., *TrAC-Trend. Anal. Chem., 2017,* 93, 183-198) (B) Scheme depicting the use of noble metal nanostructures to support localized surface plasmon resonances (LSPRs) for SERS enhancement and approaches to achieve ultrasensitive SERS enhancement. (Lee et al, Chem. Soc. Rev., 2019,

## 1.2 Surface Enhanced Raman spectroscopy background research

Recently, various kinds of SERS platform have been developed to detect ultratrace amount of analytes. SERS platform such as metallic colloidal superstructures (Han et al., Anal. Chem., 2015, 87(9), 4821-4828) and self-assembly of plasmonic colloidosome (Phan-Quang et al., Angew. Chem. Int. Ed., 2015, 54(33), 9691-9695) using oil-in-water emulsion method enabled aqueous phase detection of analytes by the advantage of their microliter volume and large surface area. Furthermore, dropping analyte and Au nanoparticles in hydrophobic surface (Yang et al., PNAS, 2016, 113(2), 268-273) and fabricating elaborated metallic nanoparticles structures on open platform system (Wang et al., Small, 2018, 14(39), 1801623) are used for highly sensitive detection of analytes by enabling analytes in proximity to metallic surface. However, these platforms are hard to realize excellent reproducibility and stability due to the variability of metal nanoparticles (NPs) aggregation in colloidal solution and open platform often induce random adsorption of molecules onto the substrate by coffee ring phenomenon and requires pre-treatment process such as long immersion time and drying process.
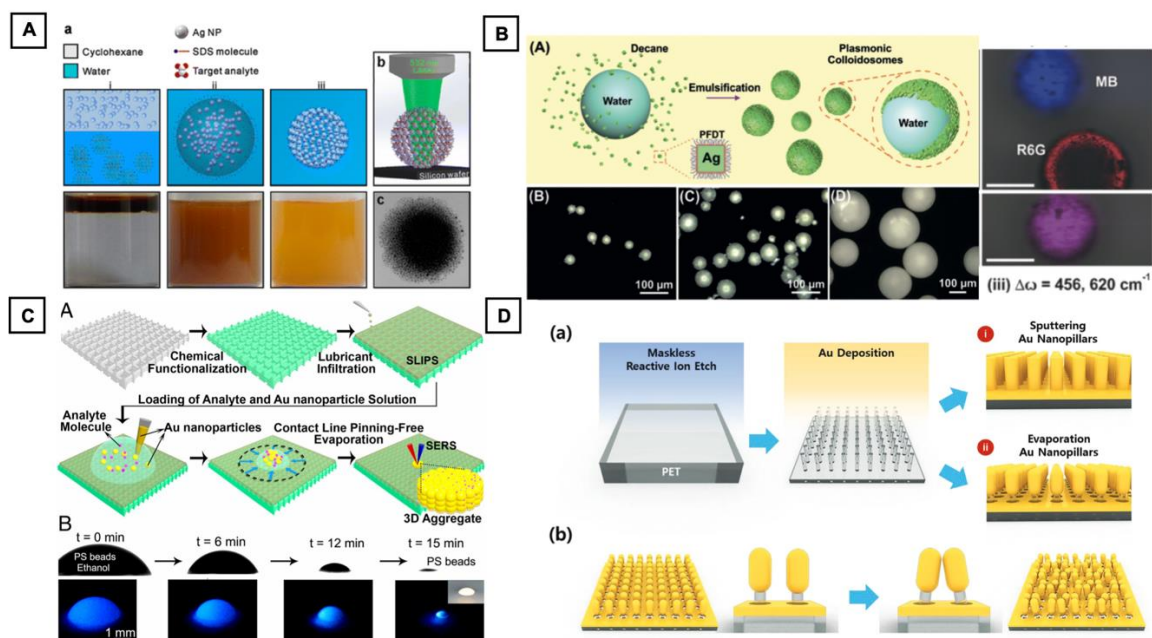


**Figure 2.** (A) Schematic and the corresponding optical images of the self-assembly of Ag NPs into spherical Ag colloidal superstructure. (Han et al., Anal. Chem., 2015, 87(9), 4821-4828) (B) Schematic illustrating the formation of plasmonic colloidosomes and microscope and SERS mapping image of colloidosome. (Phan-Quang et al., Angew. Chem. Int. Ed., 2015, 54(33), 9691-9695) (C) Scheme depicting the SLIPSERS concept to enrich analyte from common fluids. SLIPS

referring to slippery liquid-infused porous substrate. (Yang et al., PNAS, 2016, 113(2), 268-273) (D) Schematic illustrations of 3D nanopillar substrates fabrication by sputtering and thermal evaporation methods (Wang et al., Small, 2018, 14(39), 1801623)
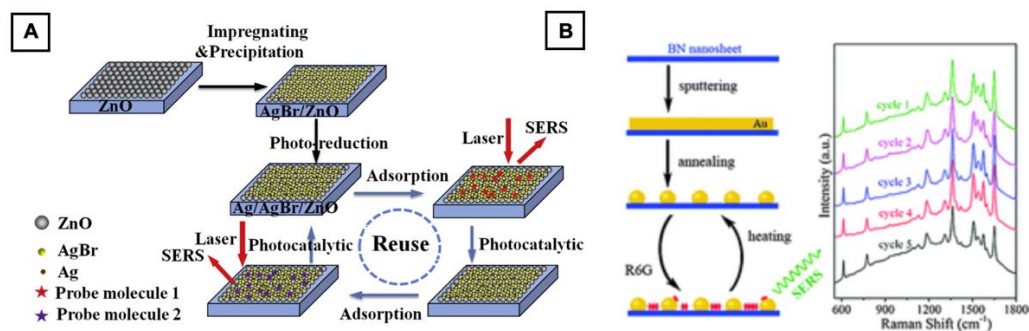


**Figure 3.** (A) Schematic illustration of reusability process of SERS substrate via photocatalytic process (Zhang et al., Spectrochim acta A., 2020, 224, 117381) and (B) annealing process (Cai et al, Phys. Chem. Chem. Phys., 2015, 17(12)

In addition, most of the SERS substrates are used as a single measurement due to the difficulty of removing the analyte completely from the substrate. Therefore, recycling processes by photocatalytic degradation under visible light irradiation (Zhang et al., Spectrochim acta A., 2020, 224, 117381) and annealing the substrate at high temperature as high as 400°C to remove adsorbed dye analyte (Cai et al, Phys. Chem. Chem. Phys., 2015, 17(12), 7761-7766) (Bu et al., 2017, Microchim. Acta, 184(8), 2805-2813) have been widely used. However, these processes partially improved the reusability of the SERS substrate in that the irradiation time of UV and visible light is long, and high temperature is required to remove the entire analytes on the substrate.
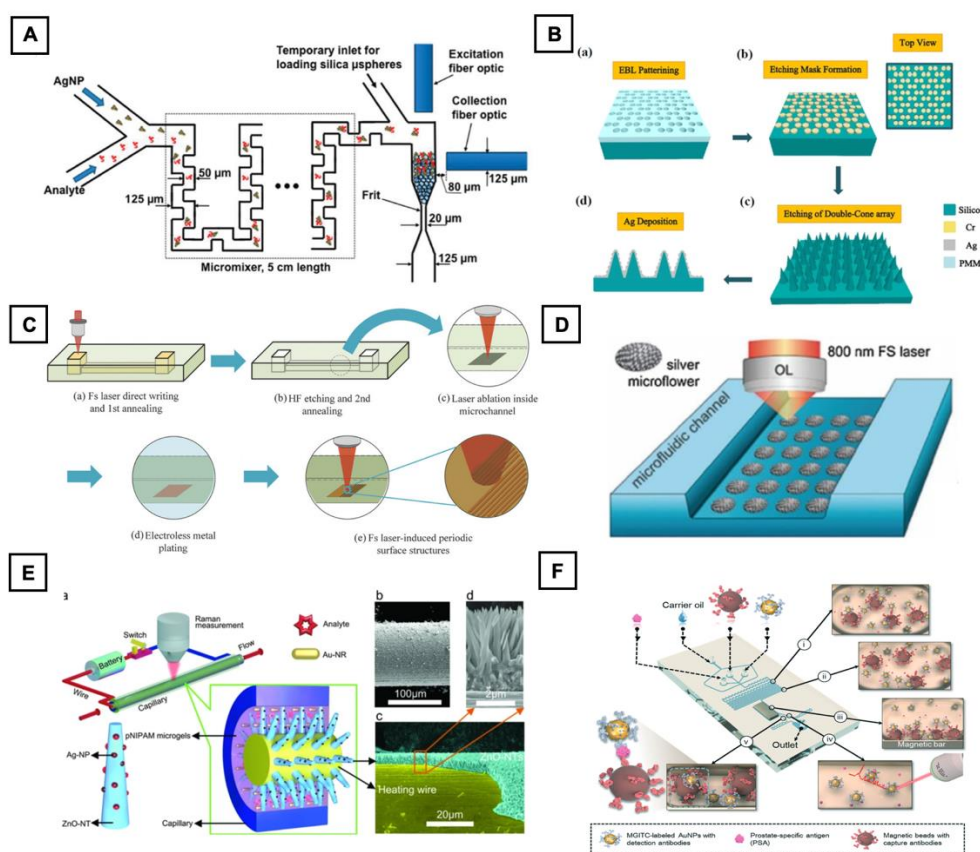
**Figure 4.** SERS platforms in microfluidic device. (A) Optofluidic SERS microfluidic system by mixing silver nanoparticles and analytes for SERS detection. (Yazdi et al., Anal. Chem., 2013, *84*(18), 7992-7998). (B) Fabrication process of SERS substrates by EBL (Mehrvar et al., Sci. Rep., 2011, 1, 12106). (C) 3D microfluidic SERS chip fabricated by all-femtosecond-laser-processing (Bai et al., Adv. Funct, Mater., 2018, 28(23), 1706262). (D) Fabrication of silver microflower array inside microfluidic device. (Xu et al., Chem. Commun., 48, 1680-682). (E) Battery-controlled composite SERS-based fluidic system and characterizations (Zhou et al., Sci. Rep., 2015, 5, 12865). (F) Enabling reusable SERS platform by magnetic immunoassay combined with droplet-based microfluidics having five compartments (Gao et al., Lab chip, 2016, 16(6), 1022-1029).

To overcome this problem, integrating SERS-active substrate with microfluidic platform has been proposed. The microfluidic SERS system has an unparalleled advantage compared to existing platforms in that it requires very small amounts of analytes in nanoliter, and the Raman signal is continuously analyzed in a closed PDMS device, preventing exposure to harmful substances and analyzing various targets in real-time. Methods such as injecting metal nanoparticles and analytes together in a sophisticated designed channel (Yazdi et al., *Anal. Chem.*, 2013, *84*(18), 7992-7998) require precise control of mixing time, and flowing the analytes into channels decorated with SERS active metal substrate via electron beam lithography (EBL) (Mehrvar et al., Sci. Rep., 2011, 1,

12106) and femtosecond laser selective metallization (FLSM) (Bai et al., Adv. Funct, Mater., 2018, 28(23), 1706262) enables discrete and delicate structures of NPs, however, high-cost and time-consuming process are major obstacles to fabricate large amounts of SERS platforms. Furthermore, to improve the Raman sensitivity, there have been many efforts to concentrate analytes close to the metallic surface such as using thermally responsive polymers (Zhou et al., Sci. Rep., 2015, 5, 12865) and magnetic nanoparticles integrated with plasmonic metal nanoparticles (Gao et al., Lab chip, 2016, 16(6), 1022-1029) which will allow analytes enrichment within the gap of metal NPs. However, these platforms have limitations in that it requires additional stimuli such as an external magnetic field and heating sources.

## 1.3 GHB detection system background research
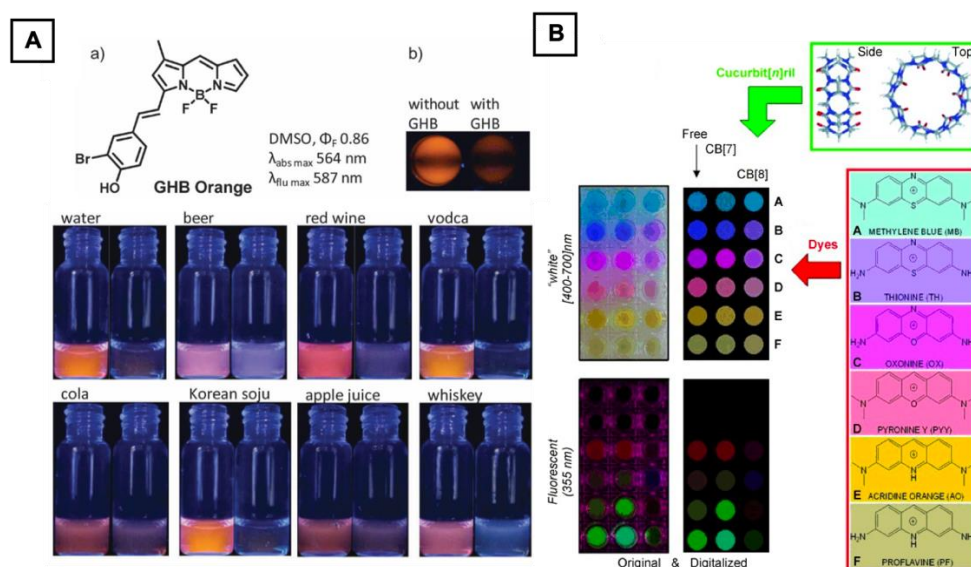


**Figure 5.** (A) Fluorescent sensor (GHB orange) (Zhai et al., ChemComm, 2014, 50(22), 2904-2906) and (B) Colorimetric sensor array (Bamues et al., Chem. Eur. J., 2009, 16(15), 4489-4495) for GHB detection.

The γ-hydroxybutyric acid (GHB), has been illegally used as a date rape drug due to its sedative effects that induce lack of awareness and unconsciousness and this effect is further amplified when consumed with alcohol. The detection of GHB is difficult because of its odorless and colorless physical properties as well as short half-life and complete excretion from the body via urine. The analysis and identification of GHB in a variety of analytical methods have been developed. However, most of the methods need pretreatment, long analysis time, and significant manipulation of the original sample. For instance, the use of gas/liquid chromatography and mass spectrometry requires acidification of blood samples of the victims and extraction process for GHB detection

(Elian et al., Forensic Sci. Int., 2001, 122(1), 43-47) (McCusker et al., J. Anal. Toxicol., 1999, 23(5), 301-305) and for NMR analysis, removal of the drug from the liquid matrix prior to the analysis is essential (Defrancesco et al., Forensic sci., 2006, 59, 321). Recently, a lot of efforts have been made to directly and sensitively detect GHB in beverages such as fluorescent sensor (GHB orange) which decreases its fluorescence when GHB is added (Zhai et al., ChemComm, 2014, 50(22), 2904-2906) and colorimetric/fluorometric sensor array which shows the concentration of GHB by extracting red, green, and blue (RGB) value (Bamues et al., Chem. Eur. J., 2009, 16(15), 4489-4495). Detection of GHB in various beverages and concentration by Raman spectroscopy (Brewter et al., Drug test. Anal., 2009, 1(1), 25-31) was also conducted. However, to the best of our knowledge, there was no platform for detecting GHB using enhanced Raman scattering with plasmonic silver nanoparticles in microfluidic device. We considered detecting GHB using portable SERS platform will have a great advantage as it enables real-time and non-destructive measurements.

## 1.4 Digital micromirror device (DMD) lithography
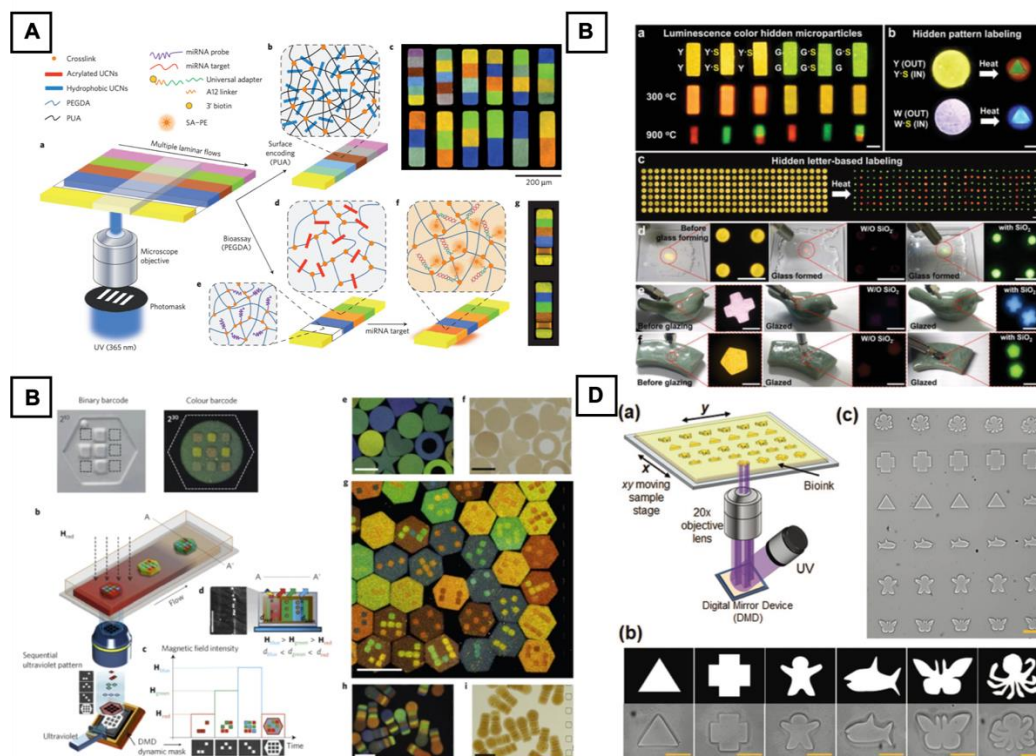


**Figure 6.** (A) Manufacturing process of microparticles having versatile information using SFL and DMD (Lee et al., Nat. Mater., 2014, 13(5), 524-520). (B) Luminescence color changing of UCN embedded microparticles fabricated by maskless DMD lithography (Baek et al., Adv. Sci., 2020, 2000104). (C) Fabrication of single material-based color barcoded magnetic nanoparticles by utilizing DMD and microfluidic device (Lee et al, Nat. Mater., 2010, 9(9), 745-749). (D)

Microfabrication of various shapes of cell laden hydrogel using DMD lithography (Hong et al. Adv. Funct., 2019, 29(13), 1808750).

In conventional photolithography, fabrication of microstructure having a desired shape and size has been mostly carried out using a transparent photomask. However, in order to fabricate various shapes and sizes of structures, it is essential to manufacture a new patterned design photomask each time. The introduction of Digital micromirror device (DMD) consisting of hundreds of thousands of micromirrors enabled direct projection of various shapes of patterned light directly on photocurable precursor solution by virtual masks controllable by simply tilting the micromirror in real-time. Various application studies are developed by combining DMD device and microlithographic equipment. The DMD-based maskless microlithography combined with computer controlled microfluidic device enabled quantitively and scalable fabrication of physiochemically identical 3D microstructures. For instance, the fabrication method via microscope-based stop flow enabled fine control of the focal point adjustment resulting in high resolution microparticles with versatile information by utilizing rare-earth UCNs (Lee et al., Nat. Mater., 2014, 13(5), 524-520), UCNs with silica nanoparticles (Baek et al., Adv. Sci., 2020, 2000104), and color barcoded magnetic nanoparticles (Lee et al, Nat. Mater., 2010, 9(9), 745-749). Furthermore, cell laden microgels with complex architecture, various size and spacing are easily fabricated on a single substrate by adjusting DMD pattern and the position of the sample stage (Hong et al. Adv. Funct., 2019, 29(13), 1808750).

## 1.5 Research Objective

In this research, we aimed to develop a highly reproducible and reusable 3D hydrogel-based SERS platform in microfluidic device by utilizing automated maskless flow microlithography technique. The physiochemically isotropic porous 3D hydrogel micro-posts arrays are constructed in the microfluidic channel using polyethylene glycol diacrylate (PEGDA) and acrylic acid (AA) precursor monomer solution by quantitatively controlling DMD patterned 365 nm UV light. A rationally designed AA branched 3D porous hydrogel network enables in-situ growth of homogeneous silver nanostructure as well as amplification of the target molecules. The 3D hydrogel SERS platform with high-density of Ag NPs demonstrated a reliable and reproducible Raman signal. Furthermore, superior reusability was verified by repeating injection process of adsorption target molecules and rinse solution. Lastly, to expand the utility of our system, a real-time detection of $\gamma$-hydroxybutyric acid (GHB), a date drug, was successfully demonstrated.

# II. EXPERIMENTAL

## 2.1 Materials

Poly(dimethylsiloxane) (PDMS, SYLGARD® 184 Silicone Elastomer Kit) was obtained from Dow corning. The poly(ethlyeneglycol) diacrylate (PEGDA, MW 700 g/mol), acrylic acid (AA), 2-hydroxy-2-methylpropiophenon (Darocur 1173), Rhodamine 6G (R6G) -Butyrolactone (GBL) were purchased from Sigma-Aldrich and used without further purification. The ethanol, methanol, silver nitrate (AgNO₃), poly(ethyleneglycol) (PEG, MW 200 g/mol), sodium hydroxide (pellet) were purchased from Daejung Chemicals & Metals. -hydroxybutyric acid (GHB) is prepared as described in the reference[6].

## 2.2 Microfluidic device preparation

PDMS microfluidic channel was fabricated though conventional soft lithography technique. Briefly, PDMS was mixed with a curing agent in a 10:1 (w/w) ratio, and degassed in vacuum for 30 min. The mixture solution was poured onto SU-8 master and cured at 65 °C for 2 hours. Glass slide was incubated in 1M NaOH solution for 1 hour, and rinsed with deionized water (DI-water). PDMS top and glass slide were treated by oxygen plasma (CUTE-1MPR, FEMTO SCIENCE) for 1 min (50 W). PDMS top was attached to glass slide and heat at 80 °C for 1 hour. 2 vol.% solution of 3-(trimethoxy) propyl acrylate in ethanol was flowed into PDMS channel and incubated for 30 min. PDMS channel was rinsed with ethanol and heated at 80 °C for 30 min in a vacuo and stored until usage.

## 2.3 Fabrication process of hydrogel micro-post array

PEGDA/AA/Ag micro-posts were fabricated with a customized DMD based mask-less photolithography system. 25 % (v/v) PEGDA, 30 % (v/v) PEG200, 30 % (v/v) DI-water, 10 % (v/v) AA were mixed with and photo-initiator (darocur 1173) by 19:1 (v/v). The precursor monomer solution was flowed into acrylated PDMS channel and crosslinked by 100 μm size circular DMD patterned 365 nm UV light (1.546 mW/cm², SOLIS-365C, Thorlabs) through 20× objective (S plan Fluor ELWD 20× DIC N1, Nikon). Hydrogel micro-posts were rinsed with di-water to remove the uncrosslinked monomer.

## 2.4 In-situ photo reduction of Ag NPs in hydrogel micro-post array in PDMS channel.

The 1.0 M AgNO$_3$ solution is flowed into PDMS channel incubated for 15 min. Subsequently, the entire hydrogel micro-posts array was irradiated with DMD patterned 365 nm UV light (4.635 mW/cm$^2$) for 1 ~ 5 min DI-water was flowed into PDMS channel and rinsed the PEGDA/AA/Ag hydrogel micro-posts for 10 min. To remove the smaller Ag NPs, 30 % (v/v) PEG200 solution was flowed into PDMS channel and rinsed for 5 min. Finally, DI-water was flowed into PDMS channel and rinsed the hydrogel-based SERS micro-posts array with DI-water for 10 min.

## 2.5 Characterization

The synthesized Ag NPs are characterized by UV−vis microspectrometry (CRAIC), and transmission electron microscopy (JEM-2100, JEOL). The Raman spectra was measured using a Raman spectroscope (alpha 300, WITec) with excitation wavelength of 633 nm, laser power of 3mW, and integration time of 1sec (20× objective lens). The 3D Raman mapping was conducted using Raman spectroscope (RAMANforce, Nanophoton) equipped with an excitation wavelength of 785 nm, laser power of 2120 kW/cm$^2$, and integration time of 6 sec (50× objective lens).

# III. RESULTS & DISCUSSION

## 3.1 Fabrication of Ag nanostructured hydrogel SERS system in microfluidic system
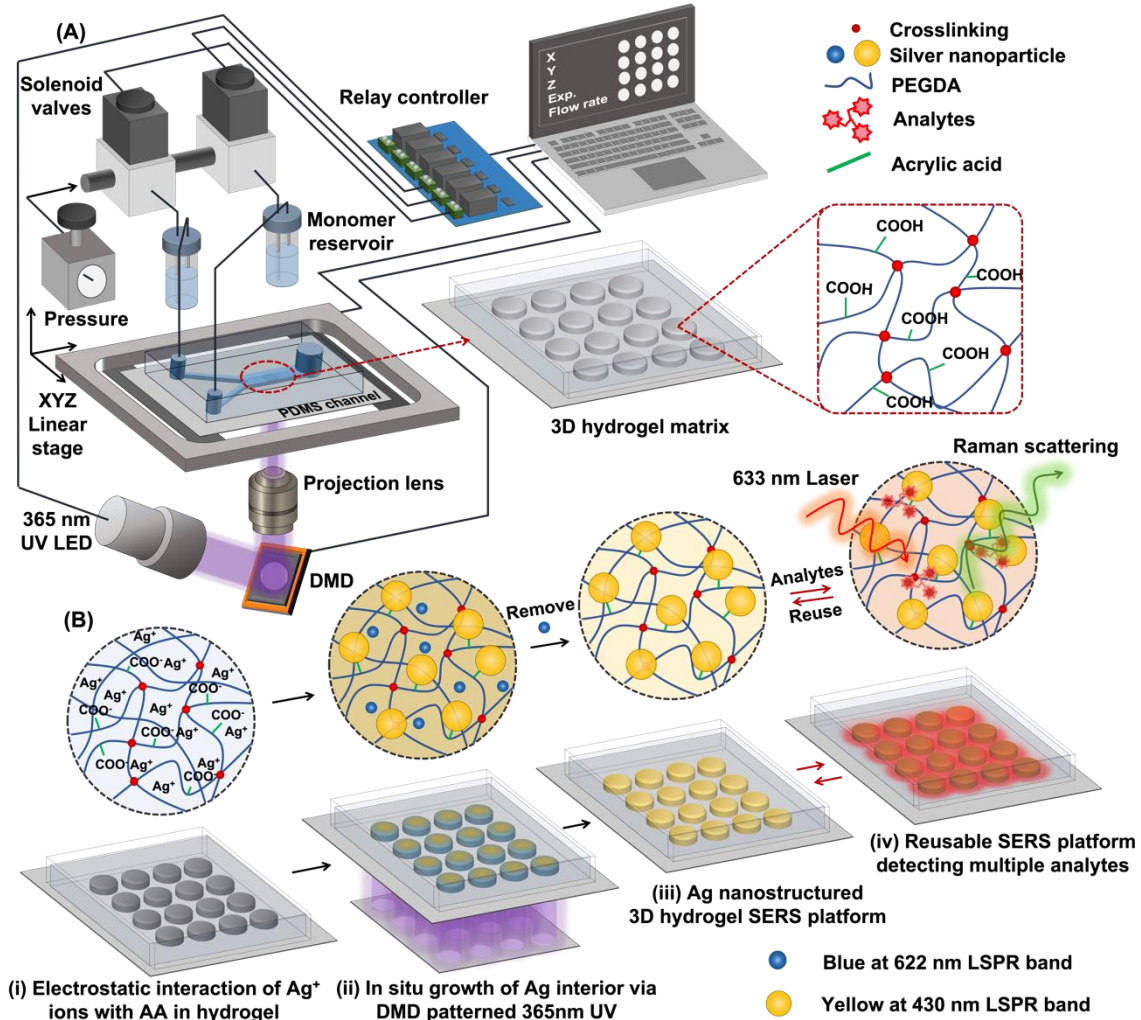


**Figure 7.** Schematic illustration of computer controlled 3D hydrogel-based SERS platform fabrication in a microfluidic device. (A) Automatic manufacturing process of physiochemically identical hydrogel microstructures with target amplification effect in microfluidic device through DMD-based maskless flow microlithograpy technique. (B) Fabrication process of reusable hydrogel-based SERS platform. (i) Electrostatic interaction between Ag ions and carboxylic groups of acrylic acid after incubation of $AgNO_3$ solution. (ii) In-situ growth of Ag NPs in hydrogel structure by photoreduction of Ag ions by 365 nm UV light. (iii) Removal of blue Ag NPs with 30 % (v/v) PEG200 solution. (iv) SERS measurement by target amplification process.

The preparation process of Ag nanostructured hydrogel SERS platform in microfluidic device is schematically illustrated in **Figure 7**. Firstly, photocurable precursor monomer solution consisting

of poly-(ethylene glycol) diacrylate (PEGDA) and acrylic acid (AA) with photoinitiator (PI) were flowed into the microfluidic channel and successively photo-polymerized to a disk-shaped microstructure by DMD patterned 365 nm UV light. (Figure 7A) High-resolution XYZ linear stage (MS-2000, ASI) and 365 nm UV LED installed DMD microlithography system (Visitech) having homogeneous beam profile enabled the fabrication of chemically and physically isotropic microstructures at the desired location in the microfluidic channel. The designated position of 3D SERS microstructure with constant pitch was controlled by programmed XYZ linear stage and 365 nm UV LED installed DMD microlithography system (**Figure 8**) by Labview software, respectively. The prepared hydrogel microstructures remained in the channel after rinsing the uncrosslinked monomers due to the silane chemical reaction allowing strong attachment to the glass substrate. Next, the 1.0M of silver nitrate ($AgNO_3$) solution was injected into the microfluidic channel by a flow rate of $1.5\ e^{-8}\ m^3/s$ (Figure 7B (i)). The carboxylic acid functional group of AA was rationally utilized to bind positively charged Ag ions ($Ag^+$) in the hydrogel network via electrostatic interaction. $Ag^+$ ions in the hydrogel network were then photo-reduced to Ag nanostructures ($Ag^0$) upon exposure to 365 nm UV irradiation (Figure 7B (ii)) and this in-situ photo-reduction process of Ag ions via computer controlled DMD patterned 365 nm UV light is very useful in that it provides a homogeneous distribution of Ag NPs within the polymer networks. To obtain the reliable SERS signal, an additional rinsing process with 30 % PEG 200 solution was applied to selectively construct homogeneous Ag nanostructures having a single LSPR band in hydrogel microstructure (Figure 7B (iii) Finally, by flowing the analyte probe solution and rinse solution alternatively into the resulted Ag nanostructured 3D hydrogel micro-posts arrays, reliable, reproducible and sensitive SERS signal are obtainable with reusable detection capability (Figure 7B (iv)).
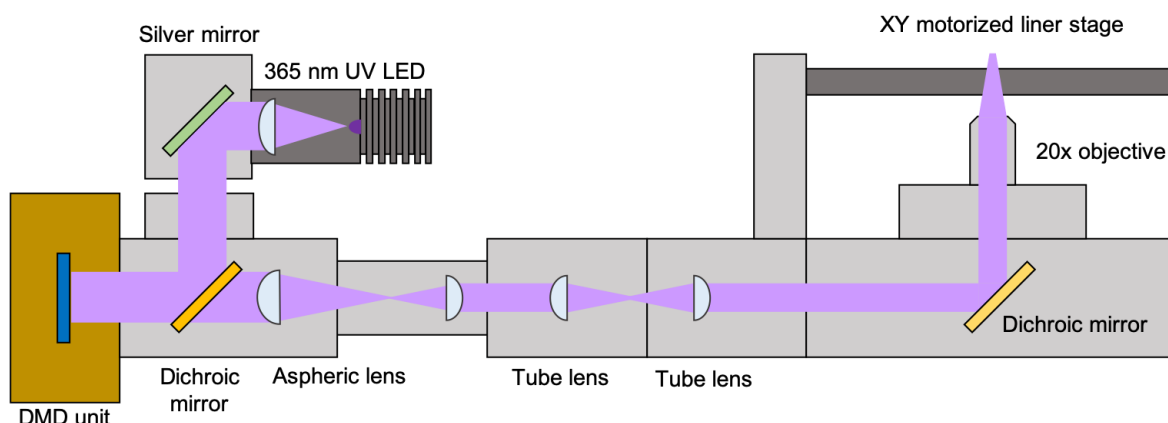


**Figure 8.** Schematic illustration of the UV LED installed DMD microlithography system.

## 3.2 Characteristics of in-situ developed Ag nanoparticles in hydrogel structure

The in-situ developed Ag nanoparticles in hydrogel micro-posts exhibited different colors according to the 365 nm UV exposure time (**Figure 9**). The hydrogel micro-posts array exhibited blue color upon exposure to 365 nm UV light for 1min, and the yellow color was further developed after 2 min exposure of 365 nm UV light. After exposure to 365 nm UV light for 5 min, these yellowish hydrogel micro-posts further changed to yellowish-brown color with two distinctive absorption bands at 430 and 622 nm associated to the localized surface plasmon resonance (LSPR) of Ag nanostructures. It is well known that LSPR bands of silver nanostructures are highly influenced by their size, morphologies, and concentration.[7, 8] Therefore, we assumed that Ag nanostructures having two different morphologies were developed at 430 and 622 nm. However, with the hydrogel structure prepared without AA, the growth of Ag NPs was not observed after 5 min 365 nm UV exposure. (**Figure 10**)
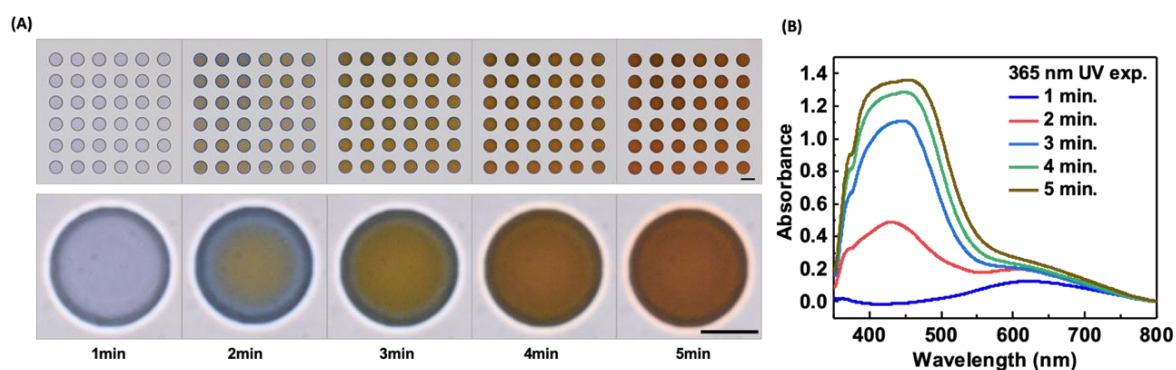


**Figure 9.** (A) Bright field images and (B) UV-Vis absorption spectra of Ag NPs hydrogel micro-posts array according to the 365 nm UV exposure time. The 4× magnification images at the top and 20× magnification images at the bottom. Scale bars are 100 μm and 50 μm, respectively.
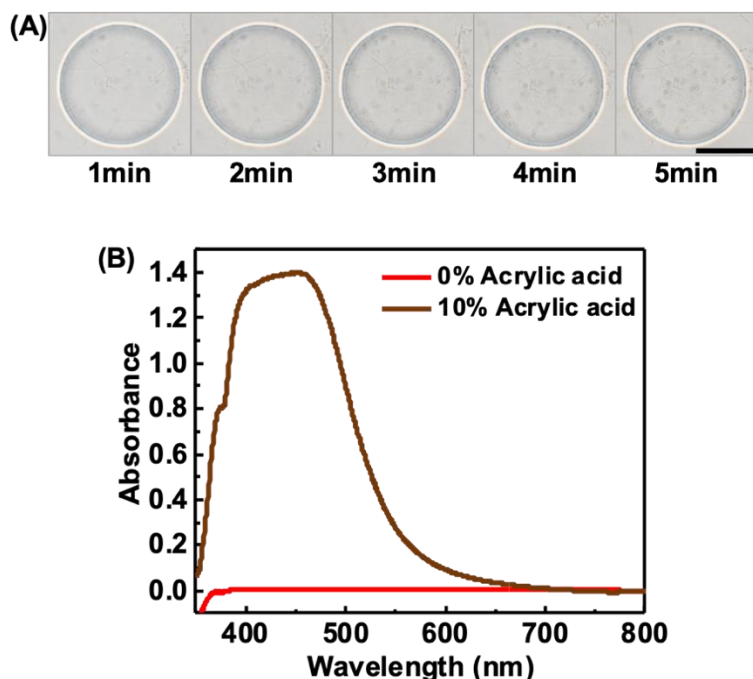
**Figure 10.** (A) Bright field optical micrographs of hydrogel micro-post fabricated without AA exposed to the UV light for a varying amount of time after infused with the metal precursor solution. (B) UV-Vis absorption spectra of PEGDA hydrogel micro-post fabricated with and without AA.

We believed that these two different morphologies of Ag NPs will induce complicated Raman scattering and reduce the reliability of the SERS detection system. The average mesh size measured for hydrogels made of the pregel solution almost identical to that used for our micro-posts was ~ 10 nm,[9] which was suitable for removing only smaller size Ag NPs. To leach out smaller Ag NPs, we used the rinsing solution – the aqueous solution containing 30 vol.% of polyethylene glycol ($M_w$ = 200 g/mol, PEG200), which is known to stabilize the dispersion of Ag NPs[10] and thus would facilitate the release of smaller size Ag NPs from the micro-posts without forming agglomerates. After rinsing with 30 % [v/v] PEG200 solution, Ag NPs of LSPR band at 622 nm was completely removed and the color of the hydrogel micro-posts array changed from yellowish brown to bright yellow (**Figure 11**A). In addition, the UV-Vis absorption spectra showed complete removal of 622 nm Ag NPs by LSPR band disappearance (Figure 11B).
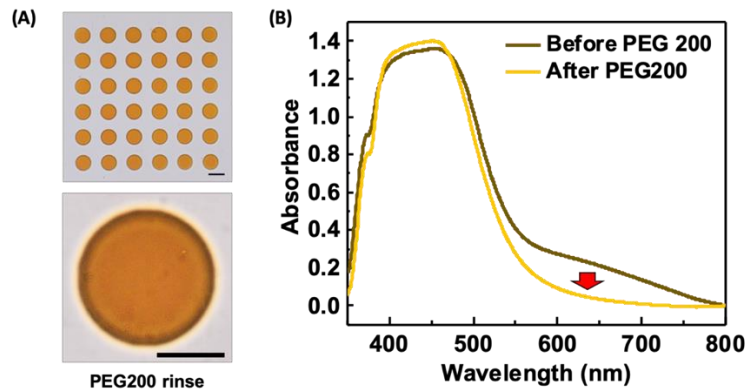
**Figure 11.** (A) Bright field images and (B) UV-Vis absorption spectra of Ag NPs hydrogel micro-posts array after rinsing with 30 vol.% PEG 200 solution in DI water. The 4× magnification images at the top and 20× magnification images at the bottom. Scale bars are 100 μm and 50 μm, respectively.
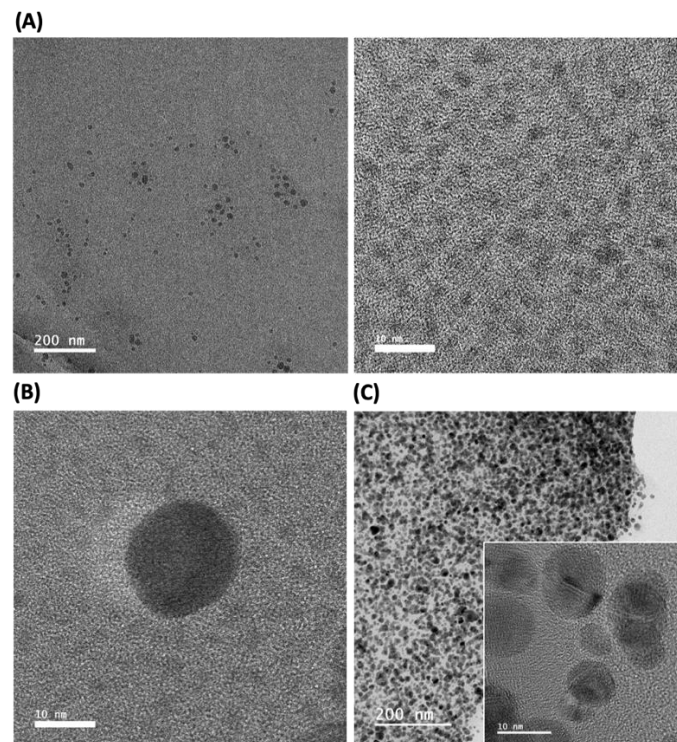


**Figure 12.** HRTEM images of (A) 1min Ag NPs with LSPR band at 622 nm, Ag NPs with LSPR band at 430 nm (B) before and (C) after rinsing with PEG200.

The characteristic of Ag NPs is further analyzed by High-resolution transmission electron microscopy (HR-TEM) images. As in HR-TEM images, Ag NPs with an average size of about ~ 2.4 nm corresponding to LSPR band at 622 nm were observed after 1 min exposure of 365 nm UV light to the PEGDA/AA micro-post (**Figure 12**A). As the UV exposure time increases, the larger

sized Ag NPs with ~ 18 nm diameter corresponding to yellow Ag NPs with 430 nm LSPR band appeared (Figure 11B) along with smaller Ag NPs. HR-TEM image obtained after rinsing the 5 min UV exposure hydrogel post with PEG200 solution. We could observe the smaller Ag NPs are completely removed after additional rinse process. The Energy-dispersive X-ray spectroscopy (EDS) spectra of each Ag NPs further demonstrates the existence of Ag NPs in hydrogel structure (**Figure 13**).
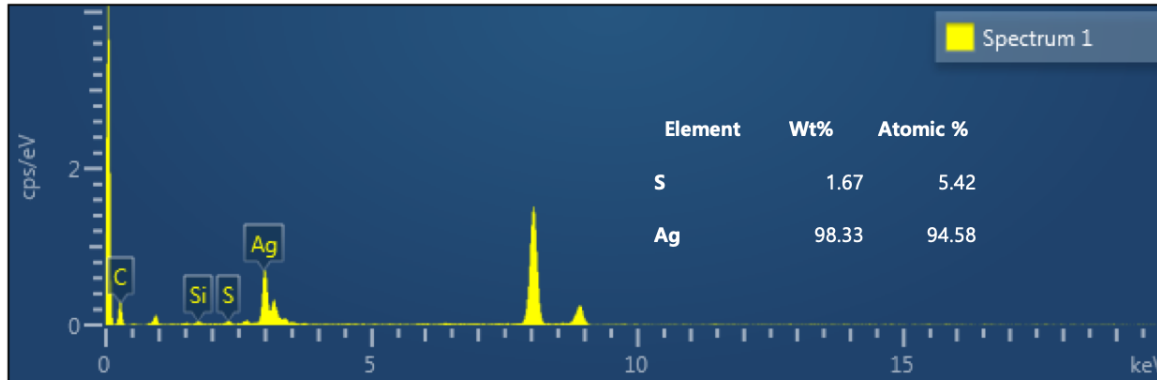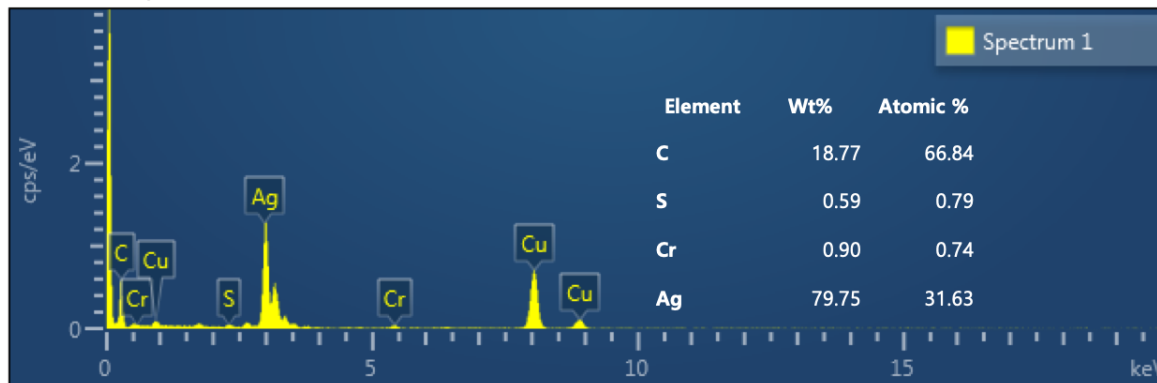


**Figure 13.** Energy-dispersive X-ray spectroscopy (EDS) spectra of hydrogel micro-posts with LSPR band at (A) 622 nm (blue Ag NPs) and (B) 430 nm (yellow Ag NPs)

## 3.3 Analyte amplification effect of hydrogel structure
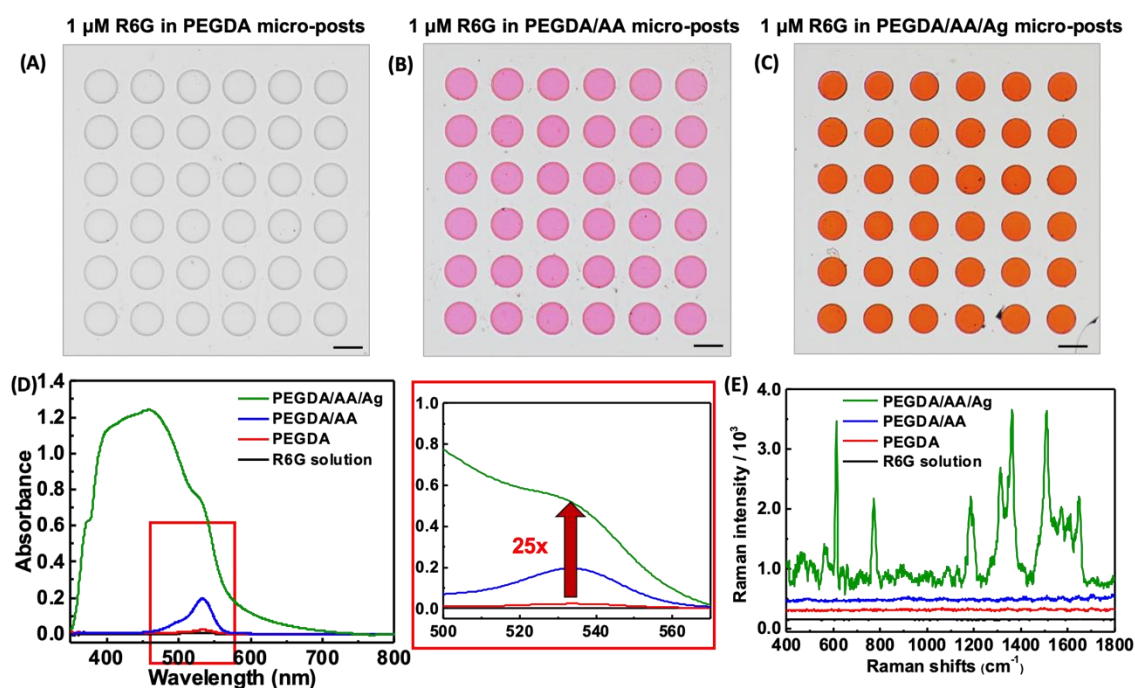


**Figure 14.** Bright-field images of (A) PEGDA, (B) PEGDA/AA and, (C) PEGDA/AA/Ag hydrogel micro-posts array immersed in 1 μM of R6G. (D) UV-Vis absorption spectra and (E) Raman shift of 1 μM of R6G solution and hydrogel micro-posts of PEGDA, PEGDA/AA, and PEGDA/AA/Ag post immersed in 1 μM of R6G.

Typically, in conventional liquid phase SERS systems, it is difficult to achieve high SERS performance due to the small number of analyte molecules proximate to the metallic nanoparticles. To overcome this limitation, we utilized acrylic acid to densify the target molecules and induce the close contact of target molecules to the plasmonic surface of Ag nanostructure in the porous hydrogel network.

First, we flowed 1 μM of R6G solution into AA free hydrogel micro-posts array (PEGDA post), AA branched hydrogel micro-posts (PEGDA/AA post), and Ag nanostructured PEGDA/AA post. The adsorption of R6G was hardly observed in PEGDA post when immersed in 1 μM of R6G (**Figure 14**A). However, PEGDA/AA post and PEGDA/AA/Ag post displayed intense red color of R6G upon immersion in 1 μM of R6G solution (Figure 14B, C). UV-Vis absorption spectra showed that the adsorption of R6G in PEGDA/AA post was increased by 10-fold than the PEGDA post without AA (Figure 14D) The higher adsorption of R6G in PEGDA/AA hydrogel micro-post is attributed to the charge properties by the carboxylic acid group of acrylic acid. Furthermore, in

case of PEGDA/AA/Ag post, the absorption at 530 nm was further increased by 2.5 times than the PEGDA/AA post, resulting in total 25 times than the PEGDA hydrogel micro-posts array.
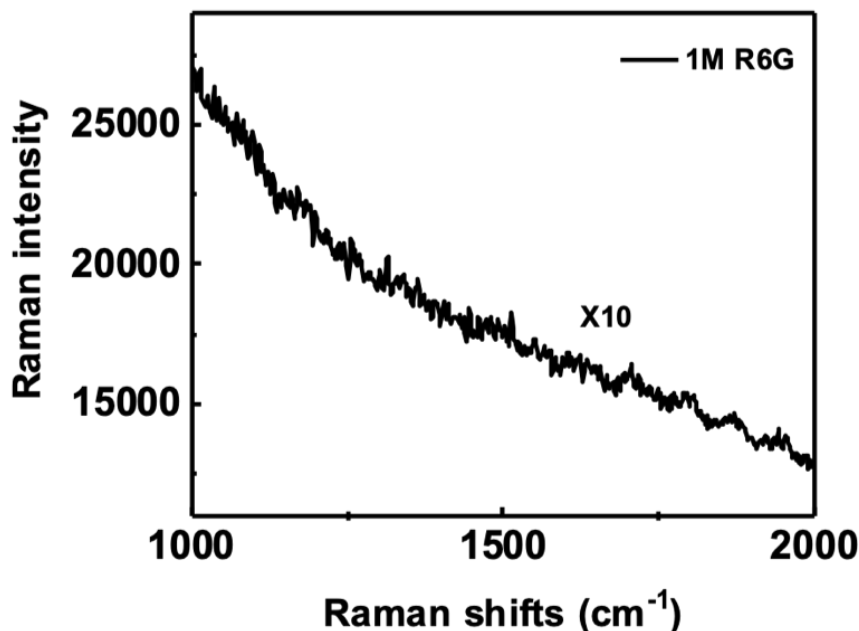


**Figure 15.** The normal Raman spectrum of aqueous $10^{-1}$ M R6G molecules adsorbed on PEGDA post enlarged by 10 times (Excitation wavelength: 633nm, Integration time: 1sec).

To confirm whether the Ag nanostructured hydrogel post have a Raman enhancement effect, Raman spectra were obtained from three different hydrogel posts using a confocal Raman spectroscopy (alpha 300S, WItec) with 633 nm excitation laser (Figure 14E). The characteristic Raman shifts of R6G was observed with PEGDA/AA/Ag post. The C-C-C ring in-plane bending at 615 cm$^{-1}$, C-H out-of-plane bending at 773 cm$^{-1}$, and aromatic C-C stretching at 1312, 1362, 1508, and 1647 cm$^{-1}$ are well consistent with the characteristic Raman signal of R6G.[11] However, without Ag NPs, the Raman peak of R6G was hard to observe until the concentration is increased to 1.0 M in PEGDA post (**Figure 15**). From these results, we concluded that high density of plasmonic Ag NPs in hydrogel structure and the AA target boosting effect near the Ag NPs surface amplified the SERS signal.

## 3.4 Sensitivity test of Raman substrate
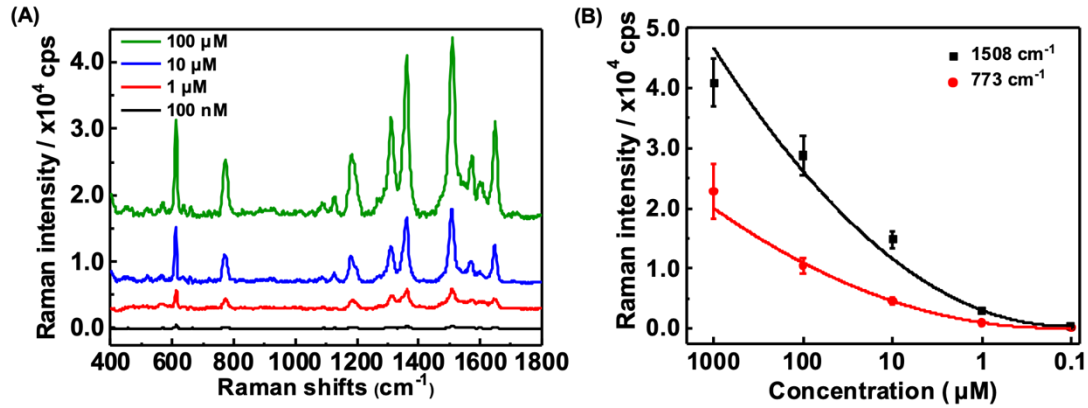


**Figure 16.** (A) Raman spectra of the PEGDA/AA/Ag micro-post array and (B) average Raman intensities measured at 773 cm$^{-1}$ and 1508 cm$^{-1}$ are shown. The error bars indicate the standard deviations calculated for measurements of 10 independent samples.

To evaluate the sensitivity of our SERS system, we measured SERS signal in various concentrations of R6G solution. The Raman spectra of R6G was measured down to 100 nM. Figure 3H shows the average Raman intensity of multiple hydrogel micro-posts array with standard deviation indicated as an error bar with Raman shifts at 773 cm$^{-1}$ and 1508 cm$^{-1}$ at various R6G concentration ranging from 1.0 mM to 100 nM. The enhancement factor of Raman intensity was calculated through the previously reported equation below.[12]

$$EF = \left(\frac{I_{SERS}}{I_{Bulk}}\right)\left(\frac{C_{Bulk}}{C_{SERS}}\right) \tag{1}$$

C$_{SERS}$ is the concentration of R6G on Ag/AA/PEGDA hydrogel micro-posts array (C$_{SERS}$ = 100 nM) and C$_{Bulk}$ is the concentration of R6G on PEGDA hydrogel micro-posts array (C$_{Bulk}$ = 1.0 M). The Raman intensity at 1508 cm$^{-1}$ of Ag/AA/PEGDA and PEGDA hydrogel micro-posts array are I$_{SERS}$ = 700.56 and I$_{Bulk}$ = 29.7, respectively. The calculated SERS enhanced factor is 2.4 × 10$^8$, which is considered higher than the typical SERS system developed so far even without pre-treatment such as heating or drying (**Table S1**).

**Table 1.** Comparisons of the substrate materials, enhancement factor of R6G, sample preparation, reusability, and targets detected between our work and previous ones.

| Substrate materials | Enhancement factor of R6G | Sample preparation | Reusability (# cycles, methods) | Targets detected | Ref # |
|---|---|---|---|---|---|
| Our work | $2.4 \times 10^8$ | Injecting analyte solution into the channel for 5 min | 20 cycles, washing with methanol for 5 min | R6G, GHB, *o*-, *m*-, *p*-ABA | |
| Boron Nitride / Ag NPs | $\sim 95 \pm 5$ | - | 30 cycles, heating at 350 °C for 5 min | R6G, rose bengal | 13 |
| Au NPs / g-carbon nitride / graphene oxide | - | Filtrating analyte solution of 2 ~ 20 ml through the substrate | 5 cycles, visible light irradiation for 130 min | R6G, 4-chlorophenol | 14 |
| Au NPs / ZnO nanorods | $1.73 \times 10^5$ | Immersion in analyte solution for 1 hour and dry before measurement | 6 cycles, UV irradiation for 100 min | R6G, erythrosine B | 15 |
| Cu substrate / Ag NPs | $1.2 \times 10^5$ | Evaporation of droplets containing Ag NPs and target analytes on the substrate | 5 cycles, immersion in DI water for 2 hours | R6G | 16 |
| Ag agarose gel | - | - | Washing with 1% trisodium citrate | 1-NAT, CV, 2-naphthoic acid, DDT | 17 |
| Ag film | $1.4 \times 10^8$ | - | 5 cycles, washing with ethanol for 30 min | R6G, 4-Mpy, 4-ATP | 18 |
| Ag / Au NPs film | $1.8 \times 10^7$ (P-ATP) | Immersion in analyte solution for 3 hours and dry before measurement | - | R6G, P-ATP, TMTD, TBZ | 19 |
| AuNPs-PEG | $9.48 \times 10^4$ | Solvent evaporation | - | R6G, methylene blue, dexketoprofen, ibuprofen | 20 |
| Si nanorods / Au NPs | $3.3 \times 10^7$ | - | - | R6G | 21 |
| Ag / reduced graphene oxide | $1.29 \times 10^5$ | Dry before measurement | - | R6G, 2,4-DNT, 4-MBA | 22 |

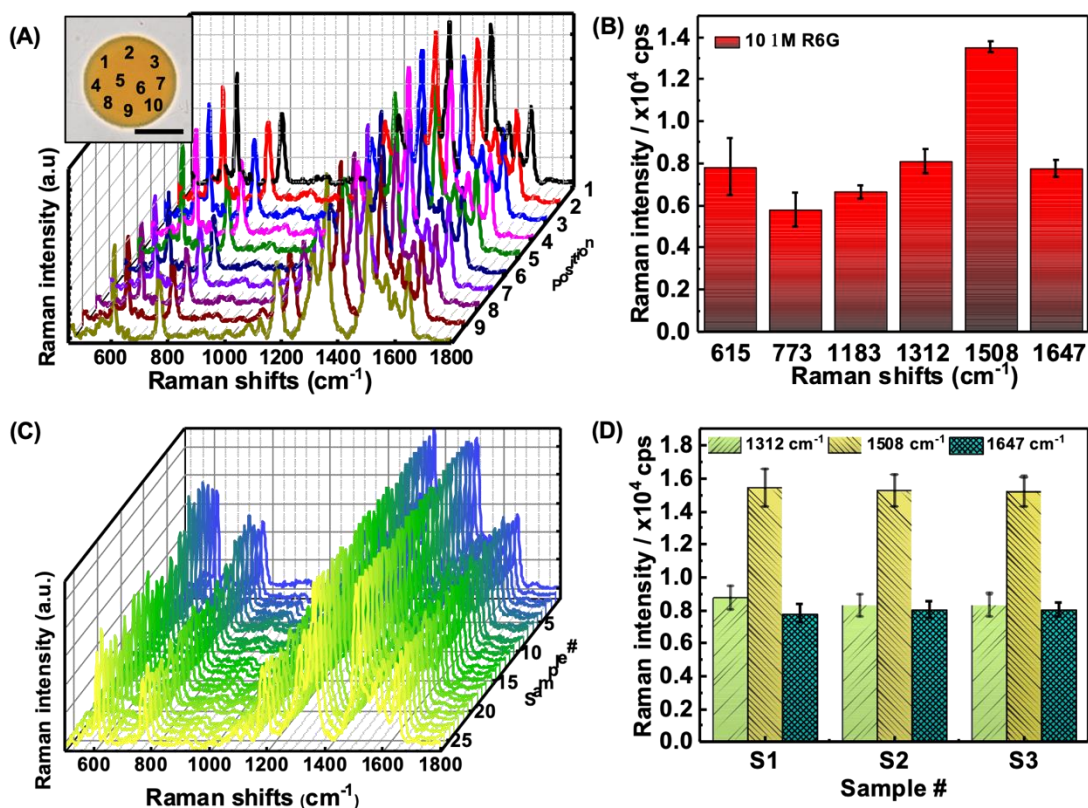## 3.5 Reproducibility and reliability of Raman substrate



**Figure 17.** The reliability and reproducibility of measurements for R6G by the PEGDA/AA/Ag micro-posts. For ten different spots within a single micro-post immersed in the 10 μM R6G aqueous solution, (A) the entire Raman spectra and (B) the standard deviations of Raman intensities measured at each peak position are shown. (C) the entire Raman spectra and (D) the standard deviations of Raman intensities calculated at three peak positions for each of three microfluidic devices were shown. For nine different spots in each of the micro-posts from three individual microfluidic devices, *i.e.* a total of 27 spots.

To examine the reliability of our SERS substrates, we compared the spot-to-spot variation in the Raman intensity measured for 10 μM R6G within the micro-post containing Ag NPs. **Figure 17**A shows Raman spectra measured at ten different locations in a single micro-post, where intensities at each Raman shifts are largely conserved. To better quantify the uniformity of Raman intensity at each principal peak position, we calculated the relative standard deviation (RSD) at each peak position (Figure 17B). The average value of RSD calculated from seven peak positions was 8.3 %.

Furthermore, the reproducibility of our SERS substrates was also examined by comparing the 10 μM R6G Raman signals from varying micro-fluidic devices. We tested three micro-fluidic devices,

and the Raman signals were measured at nine spots within an individual micro-post selected from each of three micro-fluidic devices, comparing 27 Raman spectra in total (Figure 17C). More quantitatively, the Raman intensities averaged from the nine spectra within a single micro-post were compared between three micro-fluidic devices (Figure 17D). When compared at three principal peaks, the average Raman intensities between the three micro-fluidic devices were sufficiently similar to each other, yielding 8.23 %, 6.36 % and 6.29 % of the coefficient of variations at 1312 cm$^{-1}$, 1508 cm$^{-1}$ and 1647 cm$^{-1}$, respectively. We attribute such smaller substrate-to-substrate variations to the entirely automated process used in creating SERS substrates.
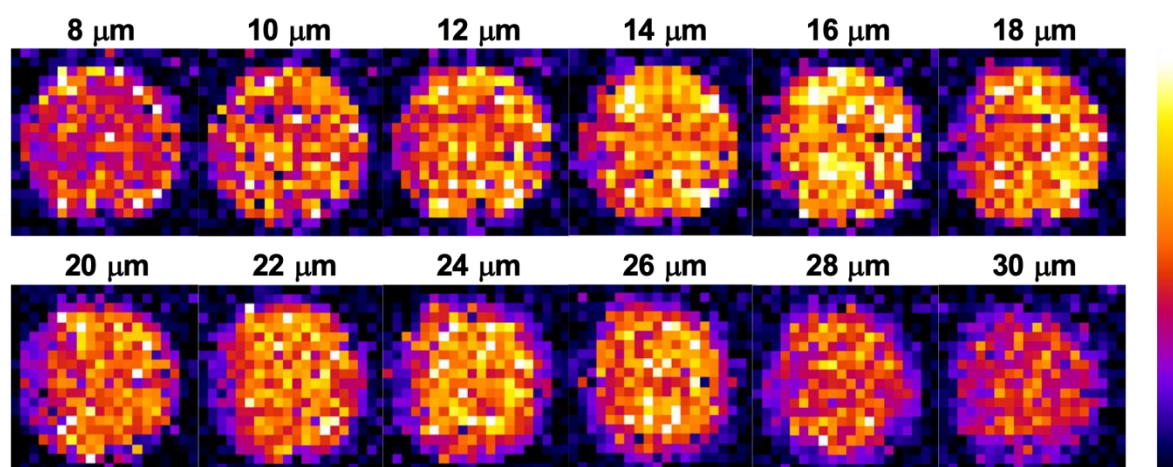


**Figure 18.** A series of in-plane mapping of the Raman intensity measured at 1508 cm$^{-1}$ along the thickness direction. A distance between adjacent in-plane mapping is 2 μm.

In addition, we conducted a 3D SERS mapping process over the entire spatial direction of the PEGDA/AA/Ag hydrogel micro-post (volume: $100 \times 100 \times 60$ μm$^3$) to identify whether the SERS substrate is Raman active in all three-dimension. **Figure 18** shows the Raman signal of R6G in a series of XY planes along the Z-direction by the circular bright illumination area. Mapping image was constructed based on Raman peak of R6G at 1508 cm$^{-1}$ band and the point to point mapping distances in X, Y, and Z directions are 5, 5, and 2 μm, respectively, resulting in a total 12000 measure points. The XY SERS mapping image highlights the strong SERS activity inside the hydrogel substrate in all layers due to the distribution of Ag NPs along with the R6G molecules. The XYZ SERS mapping results further proved the SERS effect in the entire 3D hydrogel structure by accurately representing the shape of the circular hydrogel microstructure. This result demonstrates that Ag NPs are developed in the entire volume of hydrogel structure resulting in enhanced Raman intensity.

For comparison, Raman mapping was also conducted with single PEGDA/AA hydrogel micro-

post with 10 μM R6G concentration. Mapping images of XY, YZ, and XZ planes shown in **Figure 19** are constructed based on Raman peak of PDMS at 830 cm$^{-1}$ (red) and glass slide at 1400 cm$^{-1}$ (yellow) band and the point to point mapping distances in X, Y, and Z directions are 5, 5, and 2.5 μm, respectively. As shown in the mapping image, even a very weak Raman signal of R6G was not observed with confocal Raman mapping images of 10 μM of R6G concentration in a single PEGDA/AA hydrogel micro-post. We concluded that the porous 3D hydrogel network increased the SERS hot spots density as well as the target concentration all over the substrate. As a result, this will eventually overcome the technical limitations such as spot-to-spot variations of Raman intensity on the SERS substrate.



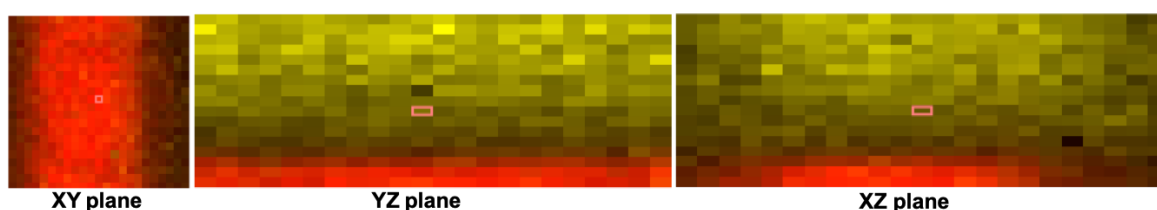**Figure 19.** Confocal Raman mapping images of 10 μM of R6G concentration in single PEGDA/AA hydrogel micro-post. Mapping images are constructed based on Raman peak of PDMS at 830 cm$^{-1}$ (red) and glass slide at 1400 cm$^{-1}$ (yellow) band. The point to point mapping distances in X, Y, and Z directions are 5, 5, and 2.5 μm, respectively. No R6G peak was observed in the hydrogel post without Ag NPs.
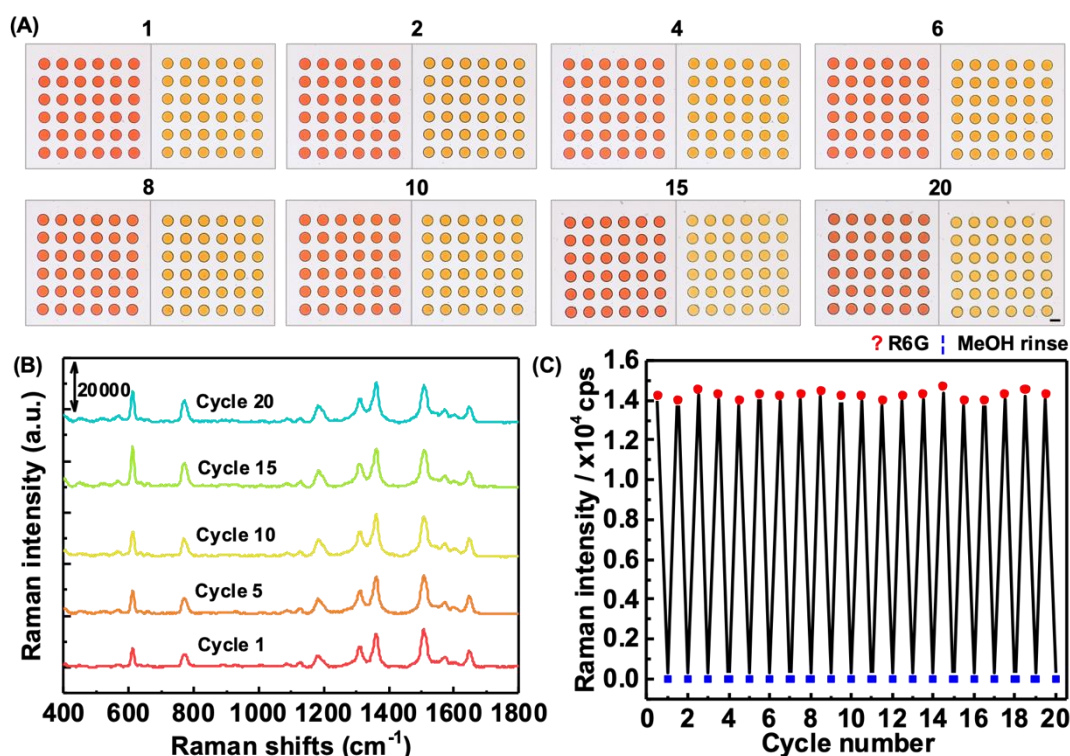
## 3.6 Reusability test of Raman substrate



**Figure 20.** The reusability, continuous multi-target sensing capability, and a demonstration of the practical application of the PEGDA/AA/Ag micro-posts. (A) Bright-field optical micrographs, (B) Raman spectra, and (C) Raman intensity measured at 1508 cm$^{-1}$ were observed as the microfluidic device was injected alternatively with the 10 μM R6G aqueous solution and the methanol – a washing solvent – for five minutes for each fluid. The cycle was repeated for 20 times consecutively. A scale bars is 100 μm.

Conventional SERS systems have focused on increasing intermolecular adsorption strength to maximize the SERS sensitivity. However, these strong interactions induce incomplete removal of target molecules from the surface of the metal nanostructures on the SERS substrate. Therefore, the practical reusability of SERS substrate has been very limited especially 3D SERS systems. To evaluate the reusability, we tested continuous immersion and rinse process of Ag nanostructured hydrogel SERS micro-posts array with R6G solution and methanol (MeOH) in PDMS channel, respectively. As in **Figure 20**A, there were almost no color change of Ag NPs hydrogel micro-posts array at each rinse cycle indicating the structure of this system is still maintained after total 20 cycles. For complete adsorption of R6G molecules on Ag NPs hydrogel micro-posts array, the R6G solution was injected for a relatively short time of 10 min at a flow rate of 1.5 e$^{-8}$ m$^3$/s, and remarkably enhanced Raman intensity is observed immediately. After Raman measurement, the adsorbed R6G molecules were completely removed from the Ag nanostructured hydrogel micro-

posts array with MeOH. The Raman spectra in Figure 20B and 20C shows that almost similar Raman signals are obtained during 20 times of R6G adsorption-desorption processes. The change in Raman intensity at 1508 cm$^{-1}$ as the infusion of R6G and MeOH at each cycle is clear enough to demonstrate the complete recycle process by R6G adsorption and desorption. As a result, despite being used several times, rapid and efficient rinsing process enables high signal reproducibility without reducing the sensitivity of the Ag NPs hydrogel micro-posts. Therefore, multiple use and high reproducibility measurement of various target molecule using our SERS substrate is expected.

### 3.7 Continuous detection of multiple targets

The reusability was further examined by measuring Raman signals of multiple analytes in a sequence. Structural isomers of the aminobenzoic acid (ABA), *i.e. o-*, *m-*, and *p-*ABA, were successively measured by our SERS substrates with an intermittent rinsing step using the methanol. When washed with the methanol, our SERS substrates fully recover the pristine state, whereas the degree to recover the pristine state was insufficient for other solvents such as ethanol and water (**Figure 21**A). SERS spectra of the three isomers were clearly differentiated without traces of former analytes, which demonstrated the reusability as well as the multi-target applicability (Figure 21B).
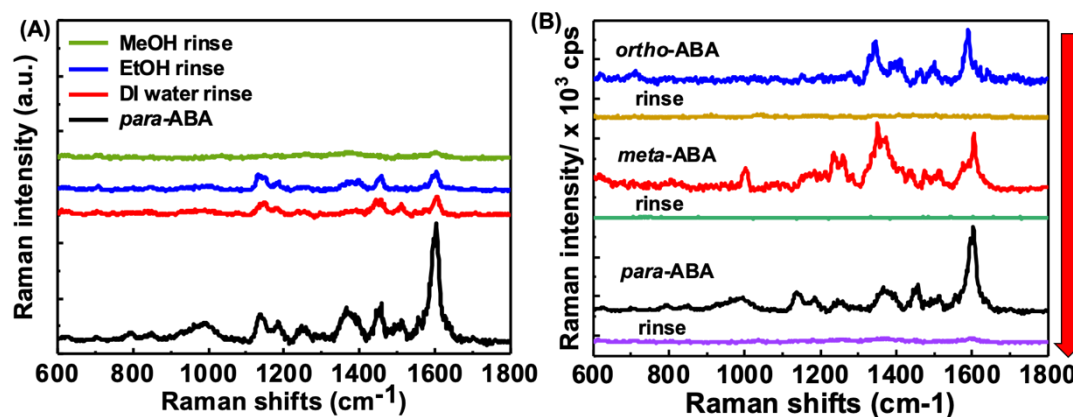


**Figure 21.** (A) The effect of washing solvent on recovering the pristine state of the PEGDA/AA/Ag micro-post after the initial measurement of *p-*ABA. (B) Sequential and continuous measurements of *o-*, *m-*, and *p-*ABA with the intermittent washing by the methanol. The order of measurement is downward.

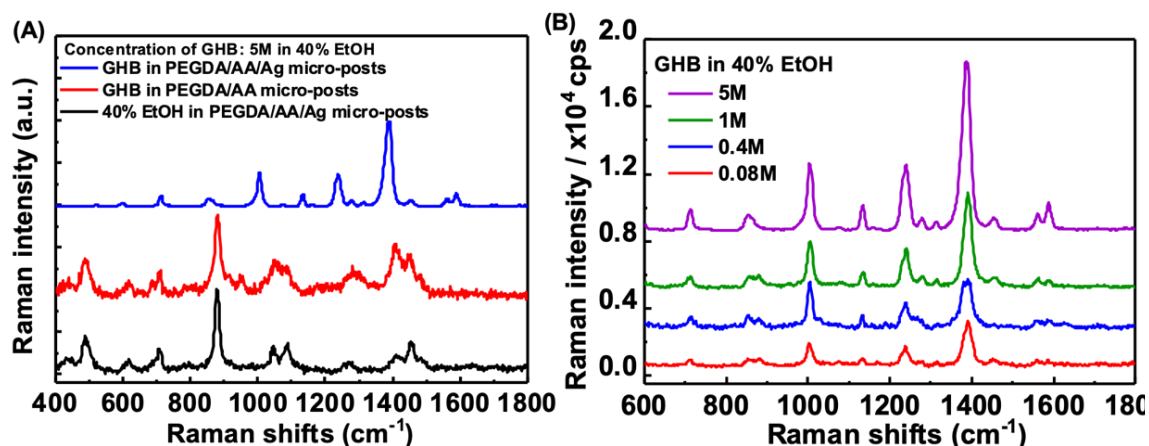## 3.8 Practical usage by detecting date rape drug



**Figure 22.** (A) SERS spectra of GHB (5.0 M) and 40 % EtOH in PEGDA/AA/Ag micro-posts and Raman spectra of GHB (5.0 M) in PEGDA/AA micro-posts. (B) The Raman spectra of the PEGDA/AA/Ag micro-posts for a varying concentration of GHB in the ethanol solution.

To expand the practical utility of our SERS system, we conducted the detection of γ-hydroxybutyric acid (GHB), one of the well-known date rape drug. GHB has been illegally used due to its sedative effects that induce lack of awareness and unconsciousness, and this physiological effect is often amplified when used with alcohol.[23] We first measured the Raman signal of 40 % ethanol (EtOH) solution, and 5 M of GHB in the presence of 40 % alcohol using PEGDA/AA/Ag micro-posts array to confirm the characteristic Raman shifts of GHB. The Raman shifts were observed at 883,1050, 1093, 1277, and 1454 cm$^{-1}$ for 40 % of EtOH. In case of PEGDA/AA/Ag hydrogel immersed in 5M of GHB solution, characteristic Raman shift of GHB at 711, 855, 1004, 1236, 1391, 1452, and 1585 cm$^{-1}$ were successfully observed in the presence of 40 % EtOH (**Figure 22**A).

It has been known that the common dosage of GHB is between 2 and 4 grams in 150-200 mL beverage.[24] Therefore, we set the minimum concentration of GHB as 0.08 M (10 mg/ml) in 40 % EtOH solution. Figure 22B shows the SERS spectra of GHB in 40 % EtOH solution at the following concentration: 0.08 M, 0.4 M, 1 M, 5M. PEGDA/AA/Ag hydrogel SERS micro-posts array successfully detected GHB down to 0.08 M in the presence of 40 % EtOH. In case of PEGDA/AA hydrogel micro-posts array without Ag nanostructured interior, only the Raman signals of EtOH was observed and any characteristic Raman signal of GHB was not observed/ Consequently, we conclude that GHB existence in alcohol can be easily identified by flowing the GHB added solution into our system. These results also validate the hydrogel-based SERS system can be sufficiently applied to the real-world problems by detecting small amounts of drugs in real-

time by simply injecting the solution into the hydrogel SERS micro-post array substrate.

# IV. CONCLUSION

In summary, we have demonstrated a highly reproducible and reusable 3D hydrogel-based SERS platform in microfluidic device. The scalable measurement was available by fabricating physiochemically isotropic hydrogel micro-posts arrays in a microfluidic device through a precisely controlled automatic DMD-based maskless flow microlithography technique. The use of acrylic acid enabled in-situ growth of Ag NPs in hydrogel structure by photo reduction of positively charged Ag ions bound to the carboxylic acid functional via electrostatic interaction as well as target amplification effect in hydrogel network. We have achieved an enhancement factor up to $2.358 \times 10^8$ in solution state without heating or solvent evaporation resulting in a highly improved SERS system compared to prior arts thanks to the homogenous silver nanoparticle distribution and target enrichment in hydrogel structure. Reproducibility and homogeneity signal are confirmed by measuring randomly selected spots in single micro-post and multiple micro-posts by substrate-to-substrate variation, respectively. 3D SERS mapping was also conducted demonstrating uniform SERS signal throughout the entire 3D SERS substrate. Finally, we have tested multiple analytes, including the R6G, three isomers of ABA, and GHB, and observe no sign of residual signals from the former analytes, which demonstrates the practical utility. Based on this study, it is concluded that hydrogel-based microfluidic platform can open new avenues in the development of reliable SERS substrates to practically detect target analytes due to their simple fabrication process, real time detection using nano-liter scale of analytes and providing the basis of reusable microfluidic SERS systems.

# V. REFERENCE

(1)    Sharma, B.; Frontiera, R. R.; Henry, A.-I.; Ringe, E.; Van Duyne, R. P. Sers: Materials, Applications, and the Future. *Mater. Today* **2012,** *15*, 16-25.

(2)    Donnelly, T.; Smith, W. E.; Faulds, K.; Graham, D. Silver and Magnetic Nanoparticles for Sensitive DNA Detection by Sers. *Chem. Commun.* **2014,** *50*, 12907—12910.

(3)    Li, J. M.; Ma, W. F.; You, L. J.; Guo, J.; Hu, J.; Wang, C. C. Highly Sensitive Detection of Target Ssdna Based on Sers Liquid Chip Using Suspended Magnetic Nanospheres as Capturing Substrates. *Langmuir* **2013,** *29*, 6147—6155.

(4)    Huang, Y. F.; Zhu, H. P.; Liu, G. K.; Wu, D. Y.; Ren, B.; Tian, Z. Q. When the Signal Is Not from the Original Molecule to Be Detected: Chemical Transformation Ofpara-Aminothiophenol on Ag During the Sers Measurement. *J. Am. Chem. Soc.* **2010,** *132*, 9244—9246.

(5)    Li, X. H.; Chen, G. Y.; Yang, L. B.; Jin, Z.; Liu, J. H. Multifunctional Au-Coated Tio2 Nanotube Arrays as Recyclable Sers Substrates for Multifold Organic Pollutants Detection. *Adv. Funct. Mater.* **2010,** *20*, 2815—2824.

(6)    Jiménez-Pérez, R.; Sevilla, J. M.; Pineda, T.; Blázquez, M.; González-Rodríguez, J. Electrochemical Behaviour of Gamma Hydroxybutyric Acid at a Platinum Electrode in Acidic Medium. *Electrochim. Acta* **2013,** *111*, 601—607.

(7)    Willets, K. A.; Van Duyne, R. P. Localized Surface Plasmon Resonance Spectroscopy and Sensing. *Annu. Rev. Phys. Chem.* **2007,** *58*, 267—297.

(8)    Zhang, J. Z.; Noguez, C. Plasmonic Optical Properties and Applications of Metal Nanostructures. *Plasmonics* **2008,** *3*, 127—150.

(9)    Choi, N. W.; Kim, J.; Chapin, S. C.; Duong, T.; Donohue, E.; Pandey, P.; Broom, W.; Hill, W. A.; Doyle, P. S. Multiplexed Detection of Mrna Using Porosity-Tuned Hydrogel Microparticles. *Anal. Chem.* **2012,** *84*, 9370—9378.

(10)    Shkilnyy, A.; Soucé, M.; Dubois, P.; Warmont, F.; Saboungi, M.-L.; Chourpa, I. Poly (Ethylene Glycol)-Stabilized Silver Nanoparticles for Bioanalytical Applications of Sers Spectroscopy. *Analyst* **2009,** *134*, 1868—1872.

(11)    Upender, G.; Satyavathi, R.; Raju, B.; Alee, K. S.; Rao, D. N.; Bansal, C. Silver Nanocluster Films as Novel Sers Substrates for Ultrasensitive Detection of Molecules. *Chem. Phys. Lett.* **2011,** *511*, 309-314.

(12)    Phan-Quang, G. C.; Lee, H. K.; Phang, I. Y.; Ling, X. Y. Plasmonic Colloidosomes as Three-Dimensional Sers Platforms with Enhanced Surface Area for Multiphase Sub-Microliter Toxin Sensing. *Angew. Chem. Int. Ed. Engl.* **2015,** *54*, 9691—9695.

(13)    Gan, W.; Tserkezis, C.; Cai, Q.; Falin, A.; Mateti, S.; Nguyen, M.; Aharonovich, I.;

Watanabe, K.; Taniguchi, T.; Huang, F. Atomically Thin Boron Nitride as an Ideal Spacer for Metal-Enhanced Fluorescence. *ACS Nano* **2019,** *13*, 12184—12191.

(14)   Qu, L.; Wang, N.; Xu, H.; Wang, W.; Liu, Y.; Kuo, L.; Yadav, T. P.; Wu, J.; Joyner, J.; Song, Y.; Li, H.; Lou, J.; Vajtai, R.; Ajayan, P. M. Gold Nanoparticles and G-C3 N4 -Intercalated Graphene Oxide Membrane for Recyclable Surface Enhanced Raman Scattering. *Adv. Funct. Mater.* **2017,** *27*, 1701714.

(15)   Sakir, M.; Salem, S.; Sanduvac, S. T.; Sahmetlioglu, E.; Sarp, G.; Onses, M. S.; Yilmaz, E. Photocatalytic Green Fabrication of Au Nanoparticles on Zno Nanorods Modified Membrane as Flexible and Photocatalytic Active Reusable Sers Substrates. *Colloids Surf. A Physicochem. Eng. Asp.* **2020,** *585*, 124088.

(16)   Fu, P.; Shi, X.; Jiang, F.; Xu, X. Superhydrophobic Nanostructured Copper Substrate as Sensitive Sers Platform Prepared by Femtosecond Laser Pulses. *Appl. Surf. Sci.* **2020,** *501*, 144269.

(17)   Wu, Y.; Hang, T.; Komadina, J.; Ling, H.; Li, M. High-Adhesive Superhydrophobic 3d Nanostructured Silver Films Applied as Sensitive, Long-Lived, Reproducible and Recyclable Sers Substrates. *Nanoscale* **2014,** *6*, 9720—9726.

(18)   Aldeanueva-Potel, P.; Faoucher, E.; Alvarez-Puebla, R. N. A.; Liz-MarzáN, L. M.; Brust, M. Recyclable Molecular Trapping and Sers Detection in Silver-Loaded Agarose Gels with Dynamic Hot Spots. *Anal. Chem.* **2009,** *81*, 9233—9238.

(19)   Zong, C.; Ge, M.; Pan, H.; Wang, J.; Nie, X.; Zhang, Q.; Zhao, W.; Liu, X.; Yu, Y. In Situ Synthesis of Low-Cost and Large-Scale Flexible Metal Nanoparticle–Polymer Composite Films as Highly Sensitive Sers Substrates for Surface Trace Analysis. *RSC Adv.* **2019,** *9*, 2857—2864.

(20)   Karabel Ocal, S.; Pekdemir, S.; Serhatlioglu, M.; Ipekci, H. H.; Sahmetlioglu, E.; Narin, I.; Duman, F.; Elbuken, C.; Demirel, G.; Onses, M. S. Eco-Friendly Fabrication of Plasmonically Active Substrates Based on End-Grafted Poly(Ethylene Glycol) Layers. *ACS Sustain. Chem. Eng.* **2019,** *7*, 4315—4324.

(21)   Lin, D.; Wu, Z.; Li, S.; Zhao, W.; Ma, C.; Wang, J.; Jiang, Z.; Zhong, Z.; Zheng, Y.; Yang, X. Large-Area Au-Nanoparticle-Functionalized Si Nanorod Arrays for Spatially Uniform Surface-Enhanced Raman Spectroscopy. *ACS Nano* **2017,** *11*, 1478—1487.

(22)   Naqvi, T. K.; Srivastava, A. K.; Kulkarni, M. M.; Siddiqui, A. M.; Dwivedi, P. K. Silver Nanoparticles Decorated Reduced Graphene Oxide (Rgo) Sers Sensor for Multiple Analytes. *Appl. Surf. Sci.* **2019,** *478*, 887—895.

(23)   Thai, D.; Dyer, J. E.; Benowitz, N. L.; Haller, C. A. Ghb and Ethanol Effects and Interactions in Humans. *J. Clin. Psychopharmacol.* **2006,** *26*, 524—529.

(24)   Barceloux, D. G., *Medical Toxicology of Drug Abuse: Synthesized Chemicals and Psychoactive Plants*. John Wiley & Sons: Hoboken, New Jersy, 2012; pp 89.